学位論文

The feasibility and limitation of coronary computed tomographic angiography imaging to identify coronary lipid-rich atheroma *in vivo*: Findings from near-infrared spectroscopy analysis
（近赤外線スペクトロスコピーとの対比により、冠動脈 CT を用いた心筋梗塞発症リスクを高める冠動脈内脂質プラーク同定法の臨床的意義・精度の解明を目指す臨床研究）

北原　慧

Satoshi　Kitahara

熊本大学大学院医学教育部博士課程医学専攻循環器先進医療学

指導教員

野口　暉夫　客員教授

熊本大学大学院医学教育部博士課程医学専攻循環器先進医療学

片岡　有　客員准教授

熊本大学大学院医学教育部博士課程医学専攻循環器先進医療学

2023 年 3 月

学　位　論　文

論文題名　：　**The feasibility and limitation of coronary computed tomographic angiography imaging to identify coronary lipid-rich atheroma *in vivo*: Findings from near-infrared spectroscopy analysis**

(近赤外線スペクトロスコピーとの対比により、冠動脈 CT を用いた心筋梗塞発症リスクを高める冠動脈内脂質プラーク同定法の臨床的意義・精度の解明を目指す臨床研究)

著 者 名　：　北原　慧

Satoshi　Kitahara

指導教員名　：熊本大学大学院医学教育部博士課程医学専攻循環器先進医療学　野口暉夫　客員教授

熊本大学大学院医学教育部博士課程医学専攻循環器先進医療学　片岡有　客員准教授

審査委員名　：　放射線診断学担当教授　平井　俊範

心臓血管外科学担当教授　福井　寿啓

生体微細構築学担当教授　若山　友彦

総合診療・臨床疫学担当教授　松井　邦彦

２０２３年３月

The feasibility and limitation of coronary computed tomographic angiography imaging to identify coronary lipid-rich atheroma *in vivo*: Findings from near-infrared spectroscopy analysis

Satoshi Kitahara, MD[1,2)]; Yu Kataoka, MD, PhD[1)]; Hiroyuki Miura, MD[1)]; Tatsuya Nishii[3)], MD, PhD; Kunihiro Nishimura, MD, PhD, MPH[4)]; Kota Murai, MD[1,2)]; Takamasa Iwai, MD[1)], Hayato Nakamura MD[5)], Hayato Hosoda, MD, PhD[6)]; Hideo Matama, MD[1,2)], Takahito Doi, MD, PhD[1)]; Takahiro Nakashima, MD, PhD[7)]; Satoshi Honda, MD, PhD[1)]; Masashi Fujino, MD, PhD[1)]; Kazuhiro Nakao, MD, PhD[1)]; Shuichi Yoneda, MD, PhD[1)]; Kensaku Nishihira, MD, PhD[8)]; Tomoaki Kanaya, MD, PhD[9)]; Fumiyuki Otsuka, MD, PhD[1)]; Yasuhide Asaumi, MD, PhD[1)]; Kenichi Tsujita, MD, PhD[10)], Teruo Noguchi, MD, PhD[1)2)]; Satoshi Yasuda, MD, PhD[1)11)]

1) Department of Cardiovascular Medicine, National Cerebral & Cardiovascular Center, Osaka, Japan

6-1 Kishibe-shimmachi, Suita, Osaka, Japan, 564-8565

2) Department of Advanced Cardiovascular Medicine, Graduate School of Medical Sciences, Kumamoto University, Kumamoto, Japan.

1-1-1 Chuo-ku, Honjo, Kumamoto, Kumamoto, Japan, 860-8556

3) Department of Radiology, National Cerebral & Cardiovascular Center, Osaka, Japan

6-1 Kishibe-shimmachi, Suita, Osaka, Japan, 564-8565

4) Department of Preventive Medicine and Epidemiology, National Cerebral & Cardiovascular Center, Osaka, Japan

6-1 Kishibe-shimmachi, Suita, Osaka, Japan, 564-8565

5) Division of Internal Medicine, Okinawa Prefectural Yaeyama Hospotal, Ishigaki, Okinawa, Japan

584-1 Maezato, Ishigaki, Okinawa, Japan, 907-0002

6) Department of Cardiology, Chikamori Hospital, Kochi, Japan

1-1-16 Okawasuji, Kochi, Kochi, Japan, 780-8522

7) Department of Emergency Medicine, University of Michigan, Ann Arbor

500 S. State Street, Ann Arbor, MI 48109 USA

8) Department of Cardiology, Miyazaki Medical Association Hospital, Miyazaki, Japan.

1173 Oaza-Arita, Miyazaki, Miyazaki, Japan, 880-2102

9) Department of Cardiovascular Medicine, Dokkyo Medical University Hospital, Mibu, Tochigi, Japan

880 Kitakobayashi, Mibu, Shimotsuga, Tochigi, Japan, 321-0293

10) Department of Cardiovascular Medicine Graduate School of Medical Sciences, Kumamoto University, Kumamoto, Japan

1-1-1 Chuo-ku, Honjo, Kumamoto, Kumamoto, Japan, 860-8556

11) Department of Cardiovascular Medicine, Tohoku University Graduate School of Medicine, Sendai, Miyagi, Japan

1-1 Seiryomachi, Aoba-ku, Sendai, Japan 980-8574

Total word count: 3069 words

Tables and Figures: This paper includes 2 tables, 3 figures, 2 supplementary

tables, and 4 supplementary figures.

Brief title: Comparison of CCTA with NIRS for lipid-rich plaque detection

Address for correspondence:

Yu Kataoka, MD, PhD, FACC, FAHA, FESC, FJCC

Department of Cardiovascular Medicine, National Cerebral & Cardiovascular Centre, Osaka, Japan

6-1 Kishibe-shimmachi, Suita, Osaka, Japan, 564-8565

Phone: +81 6 6170 1070

E-mail: yu.kataoka@ncvc.go.jp

Abstract

Backgrounds and aims: Coronary computed tomography angiography (CCTA) non-invasively visualizes lipid-rich plaque. However, this ability is not fully validated *in vivo*. The current study aimed to elucidate the association of CCTA features with near-infrared spectroscopy-derived lipidic plaque measure in patients with coronary artery disease.

Methods: 95 coronary lesions (culprit/non-culprit=51/44) in 35 CAD subjects were evaluated by both CCTA and NIRS imaging. CT density, positive remodeling, spotty calcification, napkin-ring sign and NIRS-derived maximum 4-mm lipid-core burden index ($maxLCBI_{4mm}$) were analyzed by two independent physicians. The association of CCTA-derived plaque features with $maxLCBI_{4mm}$ ≥400 was evaluated.

Results: The median CT density and $maxLCBI_{4mm}$ were 57.7 Hounsfield units (HU) and 304, respectively. CT density (r=-0.75, p<0.001) and remodeling index (RI) (r=0.58, p<0.001) were significantly associated with $maxLCBI_{4mm}$, respectively. Although napkin-ring sign (p<0.001) showed higher prevalence of $maxLCBI_{4mm}$ ≥400 than those without it, spotty calcification did not (p=0.13). On multivariable analysis, CT density [odds ratio (OR)=0.95, 95% confidence interval (CI)=0.93-0.97; p<0.001] and positive remodeling [OR=7.71, 95%CI=1.37-43.41, p=0.02] independently predicted $maxLCBI_{4mm}$ ≥400. Receiver operating characteristic curve analysis demonstrated CT density <32.9 HU (AUC=0.92, sensitivity=85.7%, specificity=91.7%) and RI ≥1.08 (AUC=0.83, sensitivity= 74.3%, specificity= 85.0%) as optimal cut-off values of $maxLCBI_{4mm}$ ≥400. Of note, only 52.6% at lesions with one of these plaque features exhibited $maxLCBI_{4mm}$

≥400, whereas the frequency of $maxLCBI_{4mm}$ ≥400 was highest at those with both two features (88.5%, p<0.001 for trend).

Conclusions: CT density <32.9 HU and RI ≥1.08 were associated with lipid-rich plaque on NIRS imaging. Our findings underscore the synergistic value of CT density and positive remodeling to detect lipid-rich plaque by CCTA.

Key Words: coronary, computed tomography, near-infrared spectroscopy, lipid-rich plaque

Abbreviation

CAD = coronary artery disease

CCTA = computed tomography coronary angiography

CT = computed tomography

HU = Hounsfield units

IVUS = intravascular ultrasound

LCBI = Lipid Core Burden Index

$maxLCBI_{4mm}$=maximum 4-mm Lipid Core Burden Index

NIRS = near-infrared spectroscopy

PCI = percutaneous coronary intervention

QCA = quantitative coronary angiography

RI = remodeling index

Introduction

Lipid-rich plaque has been considered as an important substrate of coronary atherosclerosis causing future coronary events [1, 2]. Coronary computed tomography angiography (CCTA) non-invasively visualizes lipid-rich plaque based on its computed tomography (CT) density in addition to the presence of positive remodeling, spotty calcification and/or napkin-ring sign [3-6]. Some of these features has been shown to associate with cardiac outcomes [7, 8]. However, cut-off value of CT density associated with lipid-rich plaque is inconsistent between clinical observational studies and *ex vivo* validation ones [9-12]. In addition, *in vivo* validation study has not been fully conducted to compare CCTA images with intravascular imaging modality which has sophisticated ability for detecting lipidic plaque burden.

Near-infrared spectroscopy (NIRS) imaging enables to quantitatively evaluate lipid-rich atheroma *in vivo* [13]. It has been shown that maximum 4-mm lipid-core burden index ($maxLCBI_{4mm}$) ≥400 corresponds to lipid-rich plaque causing acute coronary syndrome [14]. Given that this measure has been already validated by pathohistological specimen of coronary artery [15, 16], this modality provides an opportunity to investigate whether CCTA-derived plaque features

accurately identify lipid-rich plaque *in vivo*. Therefore, the current study sought to elucidate the association of CCTA features with NIRS-derived lipidic plaque measure in patients with coronary artery disease (CAD).

Patients and methods

Study Population

We retrospectively analyzed 95 consecutive patients with CAD who underwent both clinically indicated CCTA and NIRS/intravascular ultrasound (IVUS) imaging prior to percutaneous coronary intervention (PCI) from August 1st 2015 to November 30th 2020 at the National Cerebral & Cardiovascular Center, Osaka, Japan (Supplementary Figure 1). Of these, the following subjects were excluded; those imaged by inadequate CCTA imaging protocol (n=13), patients with poor quality of NIRS/IVUS images (n=1), a case with in-stent restenosis lesion (n=1), (n=1), the interval between CCTA and NIRS/IVUS imaging > 3 months (n=23) and commencement or dose escalation of any lipid-lowering agents between CCTA and NIRS/IVUS imaging (n=22). As a consequence, the remaining 35 patients with 95 de novo coronary lesions were included into the current study analysis. Written informed consent was not obtained in each subject due to the

observational analysis of hospitalized patients. However, the current study was posted on the website of our institution (http://www.ncvc.go.jp/hospital/pub/clinical-research/untersuchung/untersuchung-78.html) to inform its detail and ensure that patients could refuse inclusion into the current analysis. When we contacted with participants by a mail or telephone, we explained the study subjects and then obtained informed consent. The study protocol conforms to the ethical guidelines of the 1975 Declaration of Helsinki, and it was approved by the institutional ethics committee (research project number: M30-084-02).

The Definition of Analyzed Lesions

The current study analyzed both culprit and non-culprit lesions. Culprit lesion was defined as the segment receiving PCI. Non-culprit lesion was defined as (1) its percent diameter stenosis >20% on quantitative coronary angiography and (2) the segment without any history of PCI. If multiple lesions existed in the same vessel, we analyzed individual plaques which were separated by at least 5-mm from each other.

CCTA Imaging, and Its Quantitative and Qualitative Analyses

CCTA was performed using the second and third-generation dual-source CT

(DSCT) scanners (SOMATOM Definition Flash and SOMATOM Force; Siemens Healthcare, Forchheim, Germany). Retrospective ECG-gated spiral scan with tube current modulation or prospective ECG triggered high-pitch spiral scan was selected depending on the heart rate. Further scan parameters in the second and third-generation DSCT were as follows: section collimation 2×64×0.6-mm and 2×96×0.6-mm, gantry rotation 0.275 s and 0.25 s, respectively. Automated tube current modulation (CARE Dose4D, Siemens) and automatic tube-voltage selection (CARE kV, Siemens) were used with 240-280 mAs as qualified reference tube-current time products and 120-kV as reference tube-voltage. The images were reconstructed using iterative reconstruction (SAFIRE or ADMIRE, Siemens) with 0.6-mm slice thickness and 0.3-mm increments with a medium convolution kernel (I31f or Bv40). The current CCTA imaging protocol was complied with the SCCT guidelines for performance of coronary computed tomographic angiography [17].

Plaque CT density (HU=Hounsfield units) at analyzed lesions was quantitatively measured as follows. Firstly, a total of three region-of-interest (approximately 0.5-1.0 mm^2) was placed at the site exhibiting low CT attenuation within analyzed lesions throughout visual screening of images. Secondly, CT

density at each region-of-interest was measured and then averaged. Qualitative analysis was performed to evaluate (1) remodeling index (RI), (2) spotty calcification, (3) napkin-ring sign and (4) low attenuation plaque volume. RI was assessed in multi-planar reformatted images reconstructed in long axis and short axis view of the vessel by the following formula;

RI = (cross-sectional lesion diameter) / (diameter of a proximal reference segment)

Positive remodeling was defined as RI ≥1.1 [18, 19]. Spotty calcification was defined as <3 mm on focal multiplanar reconstruction images and cross-sectional images. Napkin-ring sign was defined as a ring-like peripheral higher attenuation of the non-calcified portion of the coronary plaque. With regard to low attenuation plaque volume, low attenuation was defined as CT value < 32.9 according to our current receiver operating curve analysis. Then, low attenuation area was automatically traced at each cross-sectional image of analyzed plaques. Low attenuation plaque volume was calculated by the sum of its area across all cross-sectional images of plaques. These quantitative and qualitative analyses were performed by using software that facilitates plaque volume measurement (Ziostation2, Ziosoft, Tokyo, Japan). These CCTA analyses were conducted by

two independent researchers who were blinded to clinical characteristics (SK and HM).

NIRS Imaging

The entire target vessel requiring PCI was evaluated by NIRS/IVUS imaging as reported previously. In detail, after intracoronary administration of nitroglycerin (100-300 μg), the imaging catheter (TVC Insight™ or Dualpro™, Infraredx, Bedford, MA, USA) was automatically pullbacked from the most distal site of the target artery at a speed of 0.5 mm/sec and 960 rpm (TVC Insight™) or 2.0 mm/sec and 1800rpm (Dualpro™) [20]. Makoto® system (Infraredx, Bedford, MA, USA) was used to analyze obtained chemogram data [15]. PCI was conducted after the completion of NIRS/IVUS imaging. $MaxLCBI_{4mm}$ at culprit and non-culprit lesions was used for the analysis [21]. NIRS images were analyzed by physicians who were blinded to the clinical characteristics of the patients (SK, KM and YK).

Quantitative Coronary Angiography Analysis

Quantitative coronary angiography (QCA) analysis was performed at culprit and non-culprit lesions by using off-line commercially available software (QAngio® XA, Medis, Leiden, the Netherlands). QCA analysis included minimal lumen

diameter, percent diameter stenosis, lesion length and reference vessel diameter.

Statistical Analysis

Continuous variables were expressed as the mean ± standard deviation and compared using the t test if data were normally distributed. Non-normally distributed continuous data were summarized as the median (interquartile range) and compared using the Wilcoxon rank sum test. Categorical variables were compared using the Fisher exact test or the Chi-square test as appropriate. Spearman's rank-order correlation was used to examine the relationship of $maxLCBI_{4mm}$ with CT density and RI. Linear regression analysis was conducted to determine CCTA plaque featured associated with $maxLCBI_{4mm}$ ≥400. Significant parameters in univariable analysis were entered into multivariable one. Receiver-operating characteristic curve analyses, and calculations of sensitivity and specificity were performed to analyze the predictive ability of CT density for $maxLCBI_{4mm}$ ≥400. The best cut-off value of CT density was determined by selecting the value which maximized the sum of sensitivity and specificity. According to the published paper analyzing lipid (n=40) and non-lipid (n=15) plaques [22], the expected difference in the frequency of low attenuation plaque

is considered as 10% between these two types of plaques. A sample of 59 lesions will be required for 90% power at a two-sided alpha level of 0.05 to detect a nominal difference of 10%, assuming a standard deviation of 10%. All P-values <0.05 were considered statistically significant. All analyses were performed with JMP version 14 (SAS Institute, Cary, NC).

Results

Clinical Demographics of Study Subjects

Clinical demographics of study population are summarized in Table 1. Patients had a mean age of 65 years, 79% were male, and they had a high prevalence of risk factors (hypertension: 74%, dyslipidemia: 86%, type 2 diabetes mellitus: 34%). 77% of study subjects presented stable CAD. With regard to the use of anti-atherosclerotic medical therapies, statin was already commenced prior to CCTA imaging in most of study population (30/35=86%). Their on-treatment low density lipoprotein cholesterol was 2.20 [1.91-2.72] mmol/l.

Coronary Angiographic Features of Analyzed Lesions

Table 1 shows angiographic characteristics of analyzed lesions. The current study analyzed 95 coronary lesions which included 51 culprit and 44 non-culprit lesions.

About 67% of analyzed lesions were located within the left anterior descending artery. There were no significant differences in the location and the frequency of proximal segment of major coronary arteries between culprit and non-culprit lesions (Supplementary Table 1). As expected, culprit lesions were more likely to exhibit a greater % diameter stenosis and a longer lesion length compared to non-culprit ones (Supplementary Table 1).

CCTA and NIRS Measures

On CCTA analysis, the median CT value at analyzed lesions was 57.7 [19.8-103.0] HU and median RI was 1.00 [0.90-1.17]. Positive remodeling, spotty calcification and napkin-ring sign were observed in 35, 31, and 26% of analyzed lesions, respectively (Table 1). NIRS measures at the corresponding lesions were shown in Table 1. The median $maxLCBI_{4mm}$ was 304 [102-516], and the prevalence of $maxLCBI_{4mm}$ ≥400 was 37%. Supplementary Table 2 presents comparison of CCTA and NIRS imaging between culprit and non-culprit lesions. Predictably, culprit lesions were more likely to exhibit lower CT value and higher RI and $maxLCBI_{4mm}$ with a greater frequency of positive remodeling and napkin-ring sign (Supplementary Table 2).

Relationships between $maxLCBI_{4mm}$ and CCTA measures

Supplementary Figure 2 illustrated the relationship of $maxLCBI_{4mm}$ with CT density and RI. CT density was negatively associated with $maxLCBI_{4mm}$ (r=-0.75, *p*<0.001, Supplementary Figure 2-a), whereas RI was positively correlated to $maxLCBI_{4mm}$ (r=0.58, *p*<0.001, Supplementary Figure 2-b). Additionally, as expected, lesions exhibiting $maxLCBI_{4mm}$ ≥400 more likely to presented a lower CT density [10.3 [-2.0-29.2] HU vs. 85.3 [53.6-116.9] HU, *p*<0.001) and a larger RI [1.18 [1.05-1.35] vs. 0.95 [0.88-1.04], *p*<0.001), accompanied by a greater frequency of napkin-ring sign (51.4% vs. 11.7%, *p*<0.001), whereas the prevalence of spotty calcification was comparable between two groups (40.0% vs. 25.0%, *p*=0.13) (Figure 1, a-d).

Uni- and multivariable analysis were conducted to identify an independent CCTA-derived feature associated with $maxLCBI_{4mm}$ ≥400. Univariable analysis demonstrated that CT density, positive remodeling and napkin-ring sign predicted $maxLCBI_{4mm}$ ≥400 at coronary lesions (Table 2). On multivariable analysis, CT density and positive remodeling emerged as the independent predictor of $maxLCBI_{4mm}$ ≥400 (Table 2). Receiver operating characteristic curve analysis determined CT density <32.9 HU (AUC=0.92, sensitivity=85.7%, specificity=91.7%) and RI ≥1.08 (AUC=0.83, sensitivity= 74.3%, specificity=

85.0%) as an optimal cut-off value associated with $maxLCBI_{4mm}$ ≥400 (Figure 1, e, f). Low attenuation plaque volume defined by this cut-off value (CT density <32.9) was significantly correlated to $maxLCBI_{4mm}$ (r=0.74, *p*<0.001, Supplementary Figure 3).

The frequency of $maxLCBI_{4mm}$ ≥400 was further compared in association with two CCTA features including CT density <32.9 HU and RI ≥1.08. The frequency of $maxLCBI_{4mm}$ ≥400 was only 4.0% at lesions without any these two CT features. Even if any one CT feature existed, the proportion of $maxLCBI_{4mm}$ ≥400 was still low (=52.6%), whereas lesions with both two features exhibited the highest frequency of $maxLCBI_{4mm}$ ≥400 (88.5%, *p*<0.001 for trend) (Figure 2). Two representative cases were illustrated by Figure 3.

Discussion

CCTA has been shown as a non-invasive modality to detect lipidic plaque associated with future coronary events. However, its validation study is limited. The present study demonstrated that CT density <32.9 as well as the presence of positive remodeling were significantly associated with $maxLCBI_{4mm}$ ≥400 on NIRS, but spotty calcification and napkin-ring sign did not. Our findings indicate

the relationship of CCTA-derived plaque density and RI with lipid-rich plaque *in vivo*.

The threshold of CT density for lipid-rich plaque has been inconsistent. Motoyama, *et al*. has used CT density <30 HU as a low attenuation plaque according to the comparison of CT density with echogenicity on greyscale IVUS [11]. However, given that evaluation of ultrasonic signal intensity is subjective, this cut-off is not invariably reliable. *Ex vivo* analyses proposed 60 or 75 HU as a cut-off which corresponds to lipid-rich plaque [9]. Since the *ex vivo* condition is characterized as the absence of cardiac motion and the different settings of CT imaging, these may account for different cut-off of CT density at lipid-rich plaque compared to the aforementioned study. We observed that CT density was associated with NIRS-derived $maxLCBI_{4mm}$, and its best cut-off value for $maxLCBI_{4mm}$ ≥400 was 32.9. Recent validation studies using coronary specimens have demonstrated that the extent of $maxLCBI_{4mm}$ favourably reflects the presence of lipid-rich plaque containing necrotic core. In particular, $maxLCBI_{4mm}$ ≥400 was an independent NIRS-derived feature which enables to differentiate culprit lesions of ACS containing much lipid content from non-culprit ones [14]. Furthermore, LRP study elucidated that $maxLCBI_{4mm}$ ≥400 predicted future

coronary events [16, 23]. These findings support that the current cut-off of CT density could be more reliable compared to greyscale-IVUS-derived one.

Positive remodeling has been reported as an another morphological feature of lipid-rich plaques [24-26]. In our analysis, RI was positively correlated to $maxLCBI_{4mm}$. Of note, its cut-off value to predict $maxLCBI_{4mm}$ ≥400 was 1.08. As mentioned above, considering that $maxLCBI_{4mm}$ ≥400 is a histologically validated measure which predicts future cardiovascular events, our cut-off value may be clinically applicable to detect lipid-rich lesion. Whether this cut-off is better to predict future events requires further investigation.

While CT density and positive remodeling independently associate with $maxLCBI_{4mm}$ ≥400, its accuracy to predict lipid-rich lesion depends on the number of existing these CCTA features at coronary lesions. In particular, the presence of either one feature is not satisfactorily to predict $maxLCBI_{4mm}$ ≥400. As shown in Figure 2, 52.6% of lesions with one feature exhibited $maxLCBI_{4mm}$ ≥400 and the remaining 47.4% of those was not necessarily NIRS-derived lipid-rich plaque *in vivo*. Similar findings were reported by another study conducting intravascular imaging and histological analysis [27]. In this study, combining two IVUS-derived plaque features (plaque burden and RI) has improved c-statistics to predict

histological fibroatheroma compared to the presence of only one feature. These findings underscore concomitance of two CCTA-derived plaque features to better evaluate the presence of lipid-rich plaque.

Spotty calcification and napkin-ring sign were not independent features associated with $maxLCBI_{4mm}$ ≥400. Lipid-rich plaque is frequently accompanied by the presence of spotty calcification. However, due to the limited resolution of CCTA imaging for visualizing this speckle calcification pattern [28], it may be difficult to evaluate the relationship of CCTA-derived spotty calcification with $maxLCBI_{4mm}$. With regard to napkin-ring sign, while culprit lesions in patients with acute coronary syndrome more likely presents this feature, the sensitivity of napkin-ring sign to detect fibroatheroma *ex vivo* is only 24.4% potentially due to its subjectivity [4]. Napkin-ring sign may not be practically useful for detection of lipid-rich lesion. Recent study has reported better accuracy of whole-heart coverage CT scanner to quantify coronary plaque volume [29]. This new technology may further improve the ability of CTCA imaging to characterize plaque quantity and quality.

Several caveats should be noted. Firstly, this study is a single-center retrospective observational study. Secondly, CCTA imaging was used according

to each physician's discretion. This may cause a potential bias to select study population. Thirdly, the current study did not specifically set CT acquisition parameters (kV, and mAs) and lumen contrast concentration. However, the correlation between CT density and $maxLCBI_{4mm}$ was consistently observed in all of subgroups stratified by median value of kV, mAs and lumen contrast density, respectively (Supplementary Figure 4). Lastly, as all patients had CAD requiring PCI with a frequent use of a statin prior to CCTA imaging, it is unknown whether the current findings can be translated to the setting of primary prevention.

In conclusion, CT density <32.9 and positive remodeling were an independent determinant of $maxLCBI_{4mm}$ ≥400 measured by NIRS. Coronary lesions with one of these features are less likely to correspond to lipid-rich plaque, whereas its frequency increased at lesions with both features. Our findings highlight the importance of CT density and positive remodeling, especially concomitance of these plaque features to accurately identify lipid-rich lesion *in vivo*.

Declaration of interests: The authors declare the following financial

interests/personal relationships which may be considered as potential competing interests: Yu Kataoka has received research support from Nipro and Abbott, and honoraria from Nipro, Abbott, Kowa, Amgen, Sanofi, Astellas, Takeda and Daiichi-Sankyo. Other authors have nothing to disclose.

Financial support: none

Author contributions: SK, HM and YK were responsible for the study design and concept. TI and HN collected the patient data. YK, KM, TN, HH, HM, TD, TN, SH, MF, KN, SY, KN, TK, FO and YA performed the data cleaning. SK and KN performed the data analysis. SK and YK wrote the first draft of the manuscript with support from KT, TN supervised the project.

Acknowledgments: We acknowledge Miss Yoshiko Yoshioka for her support to collect data.

References

1. Falk E. Plaque rupture with severe pre-existing stenosis precipitating coronary thrombosis. Characteristics of coronary atherosclerotic plaques underlying fatal occlusive thrombi. *Br Heart J.* 1983;50(2):127-34. doi: 10.1136/hrt.50.2.127.

2. Virmani R, Kolodgie FD, Burke AP, Farb A, Schwartz SM. Lessons from sudden coronary death: a comprehensive morphological classification scheme for atherosclerotic lesions. *Arterioscler Thromb Vasc Biol.* 2000;20(5):1262-75. doi: 10.1161/01.atv.20.5.1262.

3. Kröner ES, van Velzen JE, Boogers MJ, Siebelink HM, Schalij MJ, et al. Positive remodeling on coronary computed tomography as a marker for plaque vulnerability on virtual histology intravascular ultrasound. *Am J Cardiol.* 2011;107(12):1725-9. doi: 10.1016/j.amjcard.2011.02.337.

4. Maurovich-Horvat P, Schlett CL, Alkadhi H, Nakano M, Otsuka F, et al. The napkin-ring sign indicates advanced atherosclerotic lesions in coronary CT angiography. *JACC Cardiovasc Imaging*. 2012;5(12):1243-52. doi: 10.1016/j.jcmg.2012.03.019.

5. Pohle K, Achenbach S, Macneill B, Ropers D, Ferencik M, et al. Characterization of non-calcified coronary atherosclerotic plaque by multi-detector row CT: comparison to IVUS. *Atherosclerosis.* 2007;190(1):174-80. doi: 10.1016/j.atherosclerosis.2006.01.013.

6. van Velzen JE, de Graaf FR, de Graaf MA, Schuijf JD, Kroft LJ, et al. Comprehensive assessment of spotty calcifications on computed tomography angiography: comparison to plaque characteristics on intravascular ultrasound with radiofrequency backscatter analysis. *J Nucl Cardiol.* 2011;18(5):893-903. doi: 10.1007/s12350-011-9428-2.

7. Feuchtner G, Kerber J, Burghard P, Dichtl W, Friedrich G, et al. The high-risk criteria low-attenuation plaque <60 HU and the napkin-ring sign are the most powerful predictors of MACE: a long-term follow-up study. *Eur Heart J Cardiovasc Imaging.* 2017;18(7):772-9. doi: 10.1093/ehjci/jew167.

8. Otsuka K, Fukuda S, Tanaka A, Nakanishi K, Taguchi H, et al. Napkin-ring sign on coronary CT angiography for the prediction of acute coronary syndrome. *JACC Cardiovasc Imaging*. 2013;6(4):448-57. doi: 10.1016/j.jcmg.2012.09.016.

9. Han D, Torii S, Yahagi K, Lin FY, Lee JH, et al. Quantitative measurement

of lipid rich plaque by coronary computed tomography angiography: A correlation of histology in sudden cardiac death. *Atherosclerosis*. 2018;275:426-33. doi: 10.1016/j.atherosclerosis.2018.05.024.

10. Komatsu S, Hirayama A, Omori Y, Ueda Y, Mizote I, et al. Detection of coronary plaque by computed tomography with a novel plaque analysis system, 'Plaque Map', and comparison with intravascular ultrasound and angioscopy. *Circ J*. 2005;69(1):72-7. doi: 10.1253/circj.69.72.

11. Motoyama S, Kondo T, Anno H, Sugiura A, Ito Y, et al. Atherosclerotic plaque characterization by 0.5-mm-slice multislice computed tomographic imaging. *Circ J.* 2007;71(3):363-6. doi: 10.1253/circj.71.363.

12. Schlett CL, Maurovich-Horvat P, Ferencik M, Alkadhi H, Stolzmann P, et al. Histogram analysis of lipid-core plaques in coronary computed tomographic angiography: ex vivo validation against histology. *Invest Radiol.* 2013;48(9):646-53. doi: 10.1097/RLI.0b013e31828fdf9f.

13. Wang J, Geng YJ, Guo B, Klima T, Lal BN, et al. Near-infrared spectroscopic characterization of human advanced atherosclerotic plaques. *J Am Coll Cardiol*. 2002;39(8):1305-13. doi: 10.1016/s0735-1097(02)01767-9.

14. Madder RD, Puri R, Muller JE, Harnek J, Götberg M, et al. Confirmation of the Intracoronary Near-Infrared Spectroscopy Threshold of Lipid-Rich Plaques That Underlie ST-Segment-Elevation Myocardial Infarction. *Arterioscler Thromb Vasc Biol.* 2016;36(5):1010-5. doi: 10.1161/ATVBAHA.115.306849.

15. Gardner CM, Tan H, Hull EL, Lisauskas JB, Sum ST, et al. Detection of lipid core coronary plaques in autopsy specimens with a novel catheter-based near-infrared spectroscopy system. *JACC Cardiovasc Imaging*. 2008;1(5):638-48. doi: 10.1016/j.jcmg.2008.06.001.

16. Waxman S, Dixon SR, L'Allier P, Moses JW, Petersen JL, et al. In vivo validation of a catheter-based near-infrared spectroscopy system for detection of lipid core coronary plaques: initial results of the SPECTACL study. *JACC Cardiovasc Imaging*. 2009;2(7):858-68. doi: 10.1016/j.jcmg.2009.05.001.

17. Abbara S, Blanke P, Maroules CD, Cheezum M, Choi AD, et al. SCCT guidelines for the performance and acquisition of coronary computed tomographic angiography: A report of the society of Cardiovascular Computed Tomography Guidelines Committee: Endorsed by the North American Society for Cardiovascular Imaging (NASCI). J Cardiovasc Comput Tomogr. 2016;10(6): 435-449. doi: 10.1016/j.jcct.2016.10.002.

18. Hoffmann U, Moselewski F, Nieman K, Jang IK, Ferencik M, et al. Noninvasive assessment of plaque morphology and composition in culprit and stable lesions in acute coronary syndrome and stable lesions in stable angina by multidetector computed tomography. J Am Coll Cardiol. 2006;47(8):1655-62. doi: 10.1016/j.jacc.2006.01.041.
19. Gauss S, Achenbach S, Pflederer T, Schuhbäck A, Daniel WG, et al. Assessment of coronary artery remodelling by dual-source CT: a head-to-head comparison with intravascular ultrasound. Heart. 2011;97(12):991-7. doi: 10.1136/hrt.2011.223024.
20. Kataoka Y, Puri R, Andrews J, Honda S, Nishihira K, et al. In vivo visualization of lipid coronary atheroma with intravascular near-infrared spectroscopy. *Expert Rev Cardiovasc Ther*. 2017;15(10):775-85. doi: 10.1080/14779072.2017.1367287.
21. Madder RD, Goldstein JA, Madden SP, Puri R, Wolski K, et al. Detection by Near-Infrared Spectroscopy of Large Lipid Core Plaques at Culprit Sites in Patients With Acute ST-Segment Elevation Myocardial Infarction. *JACC Cardiovascular Interventions*. 2013;6(8):838-46. doi: 10.1016/j.jcin.2013.04.012.
22. Marwan M, Taher MA, El Meniawy K, Awadallah H, Pflederer T, et al. In vivo CT detection of lipid-rich coronary artery atherosclerotic plaques using quantitative histogram analysis: a head to head comparison with IVUS. Atherosclerosis. 2011;215(1):110-5. doi: 10.1016/j.atherosclerosis.2010.12.006.
23. Waksman R, Di Mario C, Torguson R, Ali ZA, Singh V, et al. Identification of patients and plaques vulnerable to future coronary events with near-infrared spectroscopy intravascular ultrasound imaging: a prospective, cohort study. *Lancet.* 2019;394(10209):1629-37. doi: 10.1016/S0140-6736(19)31794-5.
24. Schoenhagen P, Ziada KM, Kapadia SR, Crowe TD, Nissen SE, et al. Extent and direction of arterial remodeling in stable versus unstable coronary syndromes : an intravascular ultrasound study. Circulation. 2000;101(6):598-603. doi: 10.1161/01.cir.101.6.598.
25. Conte E, Annoni A, Pontone G, Mushtaq S, Guglielmo M, et al. Evaluation of coronary plaque characteristics with coronary computed tomography angiography in patients with non-obstructive coronary artery disease: a long-term follow-up study. Eur Heart J Cardiovasc Imaging. 2017;18(10):1170-8. doi: 10.1093/ehjci/jew200.
26. Chang HJ, Lin FY, Lee SE, Andreini D, Bax J, et al. Coronary Atherosclerotic Precursors of Acute Coronary Syndromes. J Am Coll Cardiol.

2018;71(22):2511-22. doi: 10.1016/j.jacc.2018.02.079.
27. Puri R, Madder RD, Madden SP, Sum ST, Wolski K, et al. Near-Infrared Spectroscopy Enhances Intravascular Ultrasound Assessment of Vulnerable Coronary Plaque: A Combined Pathological and In Vivo Study. *Arterioscler Thromb Vasc Biol.* 2015;35(11):2423-31. doi: 10.1161/ATVBAHA.115.306118.
28. Burke AP, Weber DK, Kolodgie FD, Farb A, Taylor A, et al. Pathophysiology of calcium deposition in coronary arteries. *Herz.* 2001;26(4):239-44. doi: 10.1007/pl00002026.
29. Conte E, Mushtaq S, Pontone G, Li Piani L, Ravagnani P, et al. Plaque quantification by coronary computed tomography angiography using intravascular ultrasound as a reference standard: a comparison between standard and last generation computed tomography scanners. Eur Heart J Cardiovasc Imaging. 2020;21(2):191-201. doi: 10.1093/ehjci/jez089.

Figure Legends

Figure 1. Comparison of CCTA measures between analyzed coronary lesions with and without maxLCBI$_{4mm}$ ≥400 and ROC curve analysis for predicting maxLCBI$_{4mm}$ ≥400

(a) CT density

(b) Remodeling index

(c) Spotty calcification

(d) Napkin-ring sign

(e) ROC curve analysis of CT density

(f) ROC curve analysis of remodeling index

CCTA = computed tomography coronary angiography, CT = computed tomography, HU = Hounsfield unit, maxLCBI$_{4mm}$ = maximum 4-mm Lipid Core Burden Index, RI = Remodeling index, ROC = receiver operating characteristics

Figure 2. The frequency of maxLCBI$_{4mm}$ ≥400 at analyzed lesions in association with the number of CT-derived morphological features

CT = computed tomography, LAP = low attenuation plaque (= CT density <32.9), maxLCBI$_{4mm}$ = maximum 4-mm Lipid Core Burden Index, PR = positive

remodeling (= remodeling index ≥1.08)

Figure 3. Representative cases

(a) 70 years-old gentleman was hospitalized to receive elective PCI. CCTA prior to PCI visualized an intermediate stenosis at the middle segment of his LAD. In addition to low CT density (CT density = -3.7HU), positive remodeling (RI = 1.38) (red arrow), spotty calcification (arrow head) and napkin-ring sign (asterisk) were observed at this lesion. On NIRS imaging, $maxLCBI_{4mm}$ at the corresponding site was 842.

(b) 63 years-old gentleman presented silent myocardial ischemia. CCTA imaging showed mild and severe stenoses at the proximal and the middle segment of his LAD, respectively. The mild stenosis exhibited positive remodeling (RI = 1.17) (red arrow), but CT density was 86.6. NIRS imaging showed a low level of $maxLCBI_{4mm}$ (338) at this lesion.

CT = computed tomography, HU = Hounsfield units, LAD = left anterior descending artery, $maxLCBI_{4mm}$ = maximum 4-mm Lipid Core Burden Index, SB = septal branch, RI = remodeling index

Supplementary Figure Legends

Supplementary Figure 1. Patients' disposition

CAD = coronary artery disease, CCTA = coronary computed tomography angiography, IVUS = intravascular ultrasound, NIRS = near infrared spectroscopy, PCI = percutaneous coronary intervention

Supplementary Figure 2. The relationships of $maxLCBI_{4mm}$ with CCTA measures

(a) CT density

(b) Remodeling index

CCTA = computed tomography coronary angiography, CT = computed tomography, HU = Hounsfield unit, $maxLCBI_{4mm}$ = maximum 4-mm Lipid Core Burden Index

Supplementary Figure 3. The association of low attenuation plaque volume with $maxLCBI_{4mm}$

$maxLCBI_{4mm}$ = maximum 4-mm Lipid Core Burden Index

Supplementary Figure 4. The correlation between CT density and maxLCBI$_{4mm}$ in subgroups stratified by median value of CT parameters

CT = computed tomography, maxLCBI$_{4mm}$ =maximum 4-mm Lipid Core Burden Index

Table 1. Baseline clinical characteristics and Angiographic, CCTA and NIRS measures

Baseline clinical characteristics (n=35 patients)	
Age, years	65 ± 12
Male, n (%)	30 (79%)
Body mass index (kg/m^2)	23.9 (21.9-27.2)
Clinical presentation	
Stable CAD, n (%)	27 (77%)
ACS, n (%)	8 (23%)
Coronary risk factor	
Hypertension, n (%)	26 (74%)
Dyslipidemia, n (%)	30 (86%)
Type 2 diabetes mellitus, n (%)	12 (34%)
Current Smoking, n (%)	7 (20%)
Medication use	
Aspirin, n (%)	29 (83%)
P2Y12 inhibitor, n (%)	31 (89%)
Statin, n (%)	30 (86%)
Ezetimibe, n (%)	7 (20%)
β-blocker, n (%)	22 (63%)
ACE-I / ARB, n (%)	18 (51%)
Laboratory data	
eGFR (mL/min/1.73m^2)	67.3 ± 14.9
LDL-cholesterol (mmol/l)	2.20 (1.91–2.72)
HDL-cholesterol (mmol/l)	1.19 (1.06–1.40)
Triglyceride (mmol/l)	1.46 (0.96–2.27)
Hemoglobin A1c (%)	5.9 (5.5–6.5)
Angiographic findings, CCTA and NIRS measures (n=95 lesions)	
Culprit lesion, n (%)	51 (53%)
Non-culprit lesion, n (%)	44 (47%)
Location of lesions	
LAD, n (%)	64 (67%)
LCX, n (%)	10 (11%)
RCA, n (%)	21 (22%)

Proximal lesion, n (%)	43 (45%)
QCA analysis	
% diameter stenosis (%)	51.4 (31.0–71.0)
Reference diameter (mm)	3.5 ± 0.7
Lesion length (mm)	18.0 (12.3–26.5)
CCTA findings	
CT density (HU)	57.7 (19.8–103.0)
Remodeling index	1.00 (0.90–1.17)
Positive remodeling (%)	33 (35%)
Spotty calcification (%)	29 (31%)
Napkin-ring sign (%)	25 (26%)
NIRS-IVUS findings	
$MaxLCBI_{4mm}$	304 (102–516)
$MaxLCBI_{4mm}$ ≥400	35 (37%)

ACE-I = angiotensin converting enzyme inhibitor, ACS = acute coronary syndrome, ARB = angiotensin II receptor blocker, CAD = coronary artery disease, CCTA = Coronary computed tomography angiography, CT = computed tomography, eGFR = estimated glomerular filtration rate, HDL = high density lipoprotein, HU = Hounsfield units, LAD = left anterior descending artery, LDL = low density lipoprotein, LCBI = lipid core burden index, LCX = left circumflex artery, $MaxLCBI_{4mm}$ = maximum 4mm Lipid Core Burden Index, NIRS = near-infrared spectroscopy, RCA = right coronary artery, QCA = quantitative coronary angiography

Continuous data are represented as means ± standard deviation, if data were normally distributed.

Non-normally distributed continuous data were summarized as the median (interquartile range)

Table 2. Univariable and multivariable analysis for $maxLCBI_{4mm}$ ≥400

	Univariable analysis			Multivariable analysis		
	OR	95%CI	*P* value	OR	95%CI	*P* value
CT density	0.95	0.92 – 0.97	<0.001	0.95	0.93 – 0.97	<0.001
Positive remodeling	16.25	5.71 – 46.20	<0.001	7.71	1.37 – 43.41	0.02
Spotty calcification	2.00	0.81 – 4.89	0.13			
Napkin-ring sign	8.02	2.86 – 22.45	<0.001	0.45	0.07 – 2.97	0.41

CI =Confidence interval, CT = computed tomography, $maxLCBI_{4mm}$ = maximum-4mm Lipid Core Burden Index, OR = Odds ratio

Supplementary Table1. Angiographic Findings

95 analyzed lesions			
	Culprit lesion (n=51)	Non-culprit lesion (n=44)	p value
Location of culprit lesions			
LAD, n (%)	38 (75%)	26 (59%)	
LCX, n (%)	4 (8%)	6 (14%)	0.27
RCA, n (%)	9 (18%)	12 (27%)	
Proximal lesion (%)	26 (51%)	17 (39%)	0.23
QCA analysis			
% diameter stenosis (%)	68.3 (57.8–78.0)	29.9 (24.5–35.8)	<0.001
Reference diameter (mm)	3.6 ± 0.7	3.4 ± 0.8	0.19
Lesion length (mm)	21.5 (16.4–30.1)	14.1 (9.0–20.9)	<0.001

LAD = left anterior descending artery, LCX = left circumflex artery, QCA = quantitative coronary angiography, RCA = right coronary artery

Supplementary Table 2. CCTA and NIRS Measures

n=95			
	Culprit lesion (n=51)	Non-culprit lesion (n=44)	p value
CCTA findings			
CT density (HU)	28.0 (6.5–57.7)	87.8 (65.2–121.0)	<0.001
Remodeling index	1.09 (0.95–1.28)	0.95 (0.87–1.05)	<0.001
Positive remodeling (%)	8 (18%)	25 (49%)	0.002
Spotty calcification (%)	16 (31%)	13 (30%)	0.85
Napkin-ring sign (%)	22 (43%)	3 (7%)	<0.001
NIRS-IVUS findings			
$MaxLCBI_{4mm}$	418 (272–658)	156 (39–294)	<0.001
$MaxLCBI_{4mm} \geq 400$	29 (57%)	6 (14%)	<0.001

CCTA = computed tomography coronary angiography, CT = computed tomography, HU = Hounsfield units, IVUS = intravascular ultrasound, LCBI = Lipid Core Burden Index, $MaxLCBI_{4mm}$ = maximum-4mm Lipid Core Burden Index, NIRS = near-infrared spectroscopy

Figure 1.

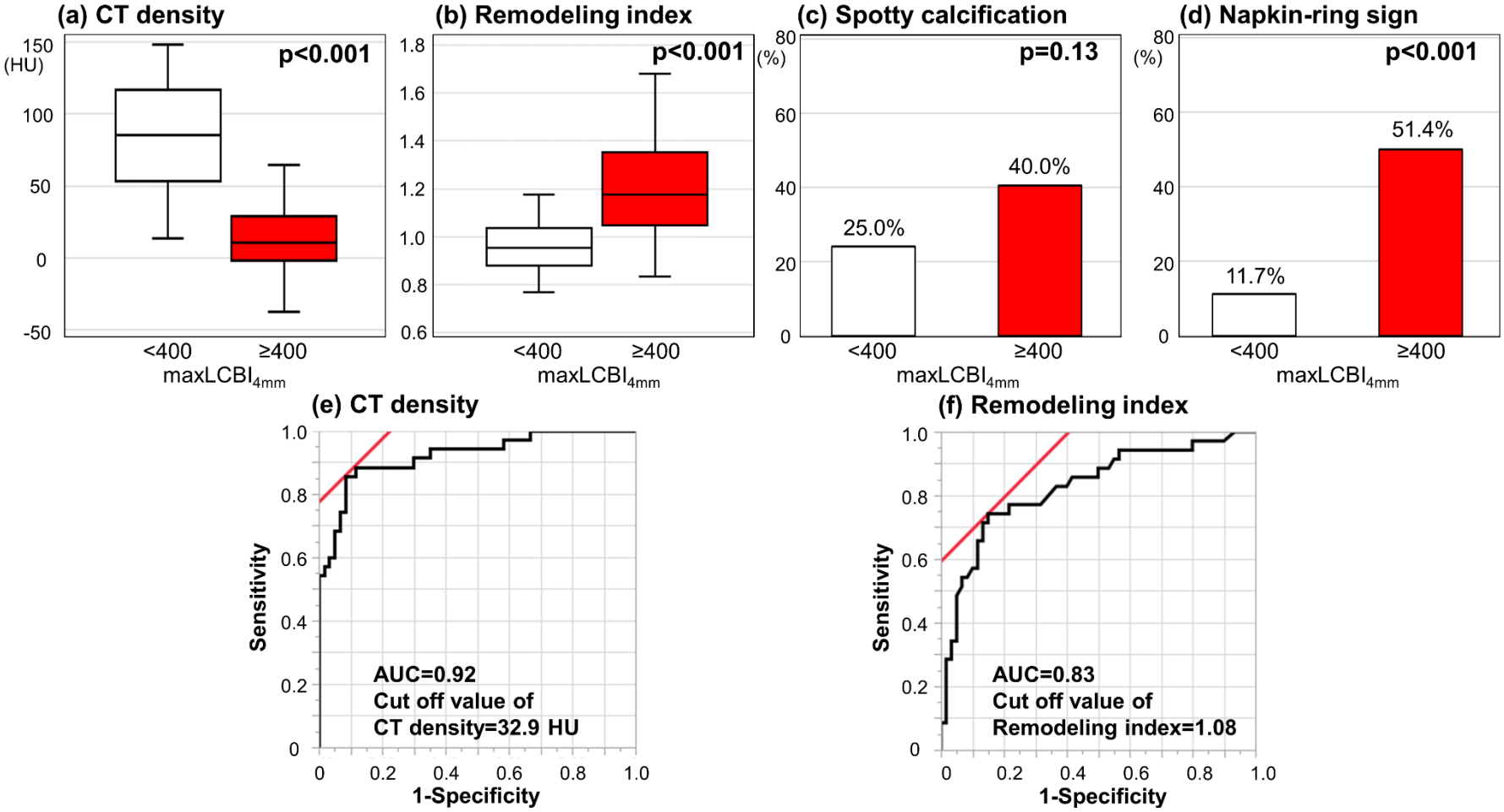
(a) CT density
p<0.001
(HU)
150
100
50
0
-50
<400
≥400
maxLCBI4mm
(b) Remodeling index
p<0.001
1.8
1.6
1.4
1.2
1.0
0.8
0.6
<400
≥400
maxLCBI4mm
(c) Spotty calcification
p=0.13
(%)
80
60
40
20
0
25.0%
40.0%
<400
≥400
maxLCBI4mm
(d) Napkin-ring sign
p<0.001
(%)
80
60
40
20
0
11.7%
51.4%
<400
≥400
maxLCBI4mm
(e) CT density
Sensitivity
1-Specificity
AUC=0.92
Cut off value of
CT density=32.9 HU
(f) Remodeling index
Sensitivity
1-Specificity
AUC=0.83
Cut off value of
Remodeling index=1.08

Figure 2.

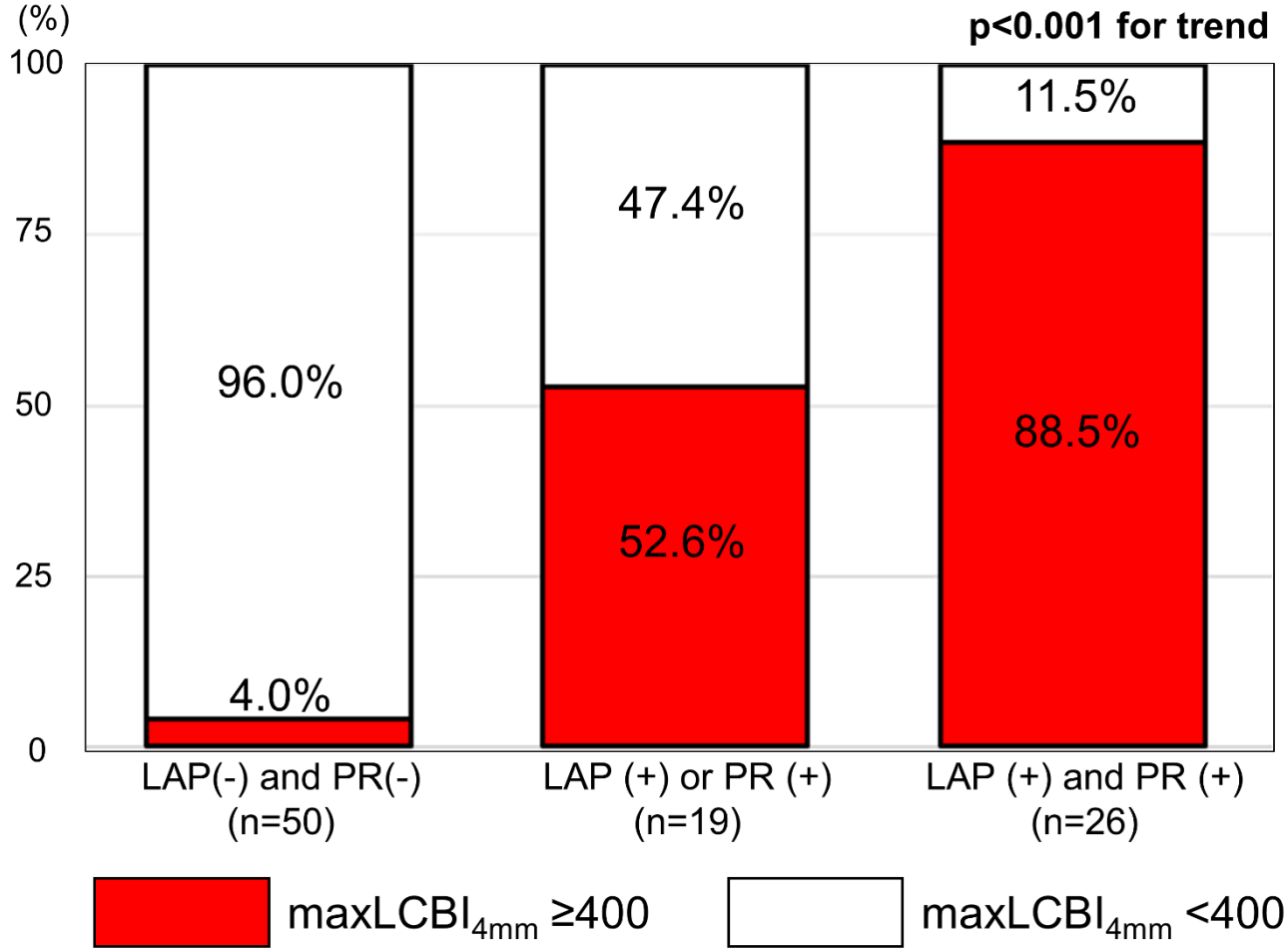
(%)
p<0.001 for trend
100
75
50
25
0
96.0%
4.0%
47.4%
52.6%
11.5%
88.5%
LAP(-) and PR(-)
(n=50)
LAP (+) or PR (+)
(n=19)
LAP (+) and PR (+)
(n=26)
maxLCBI4mm ≥400
maxLCBI4mm <400

Figure 3.

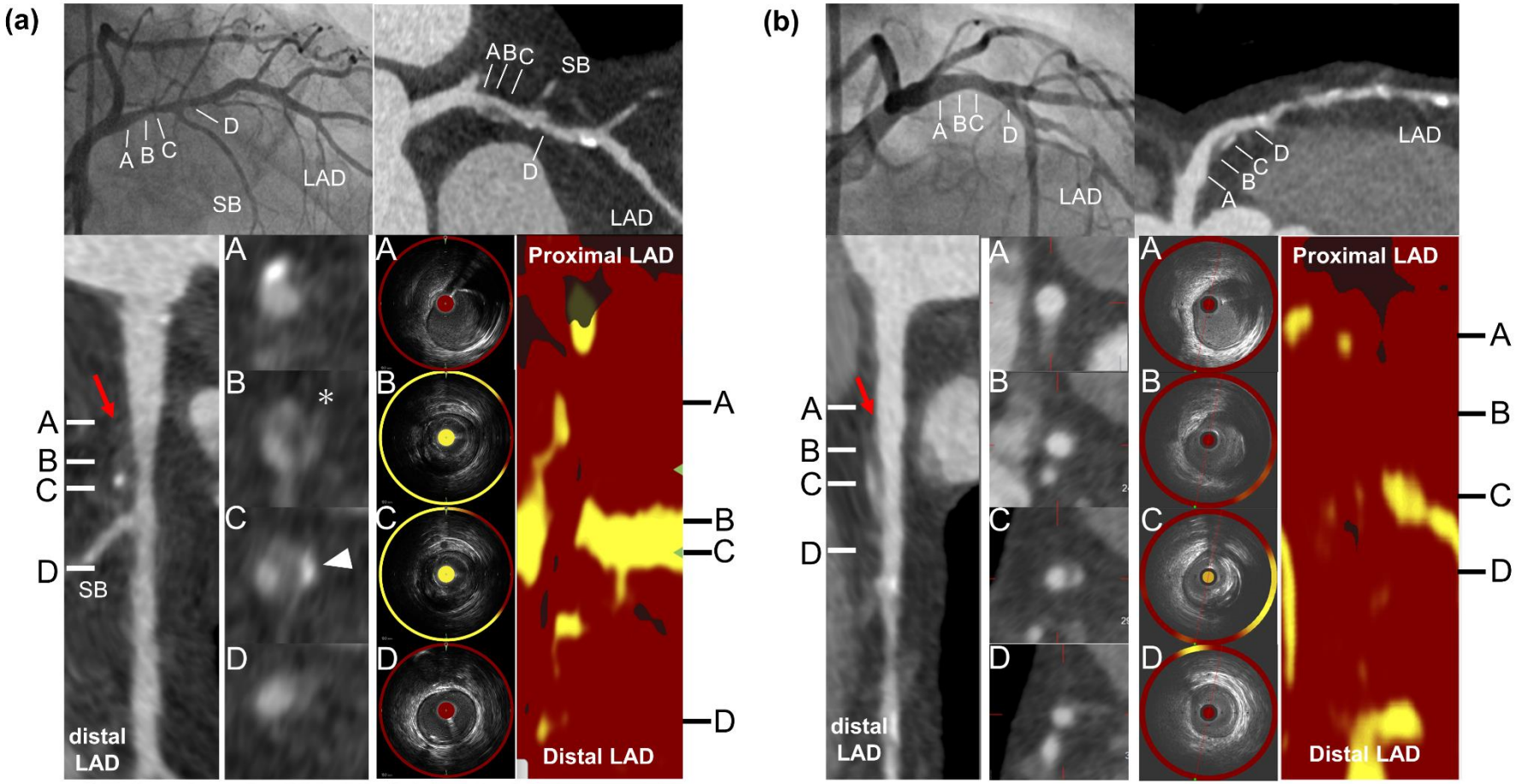

CT density=**-3.7HU**, RI=**1.38**, MaxLCBI$_{4mm}$=**842**

CT density=86.6HU, RI=**1.17**, MaxLCBI$_{4mm}$=338

Supplementary Figure 1.

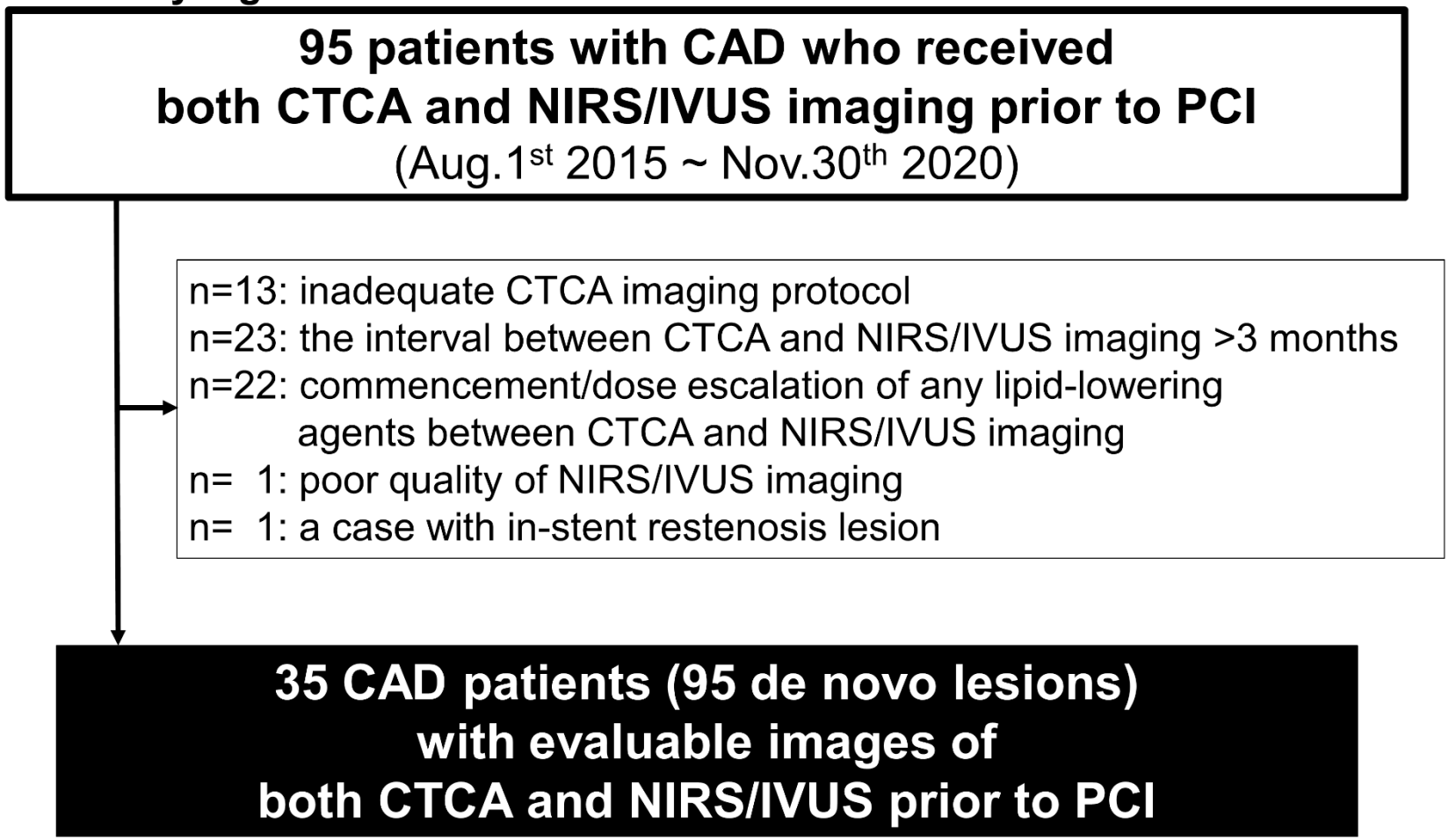

Supplementary Figure 2.

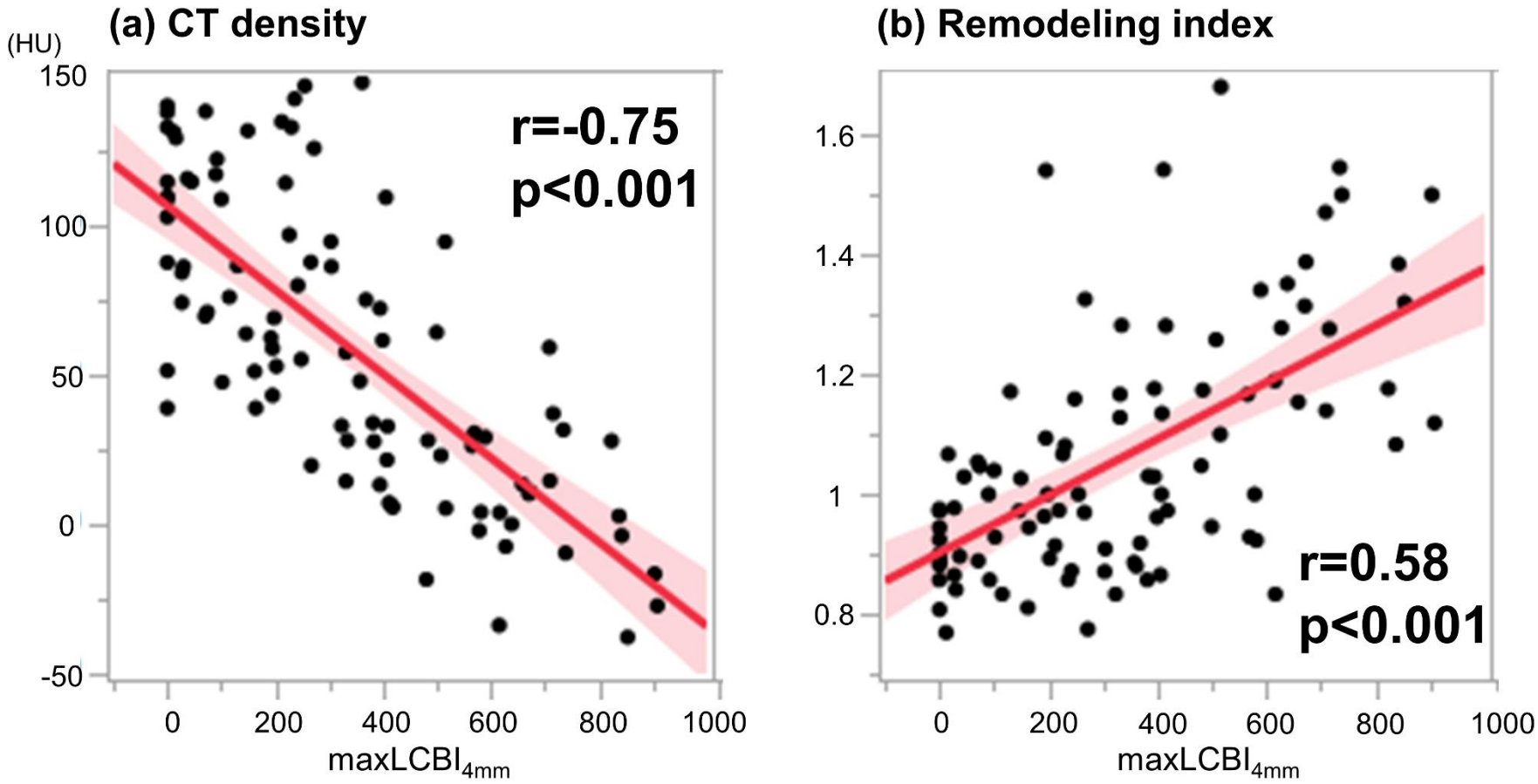

Supplementary Figure 3.

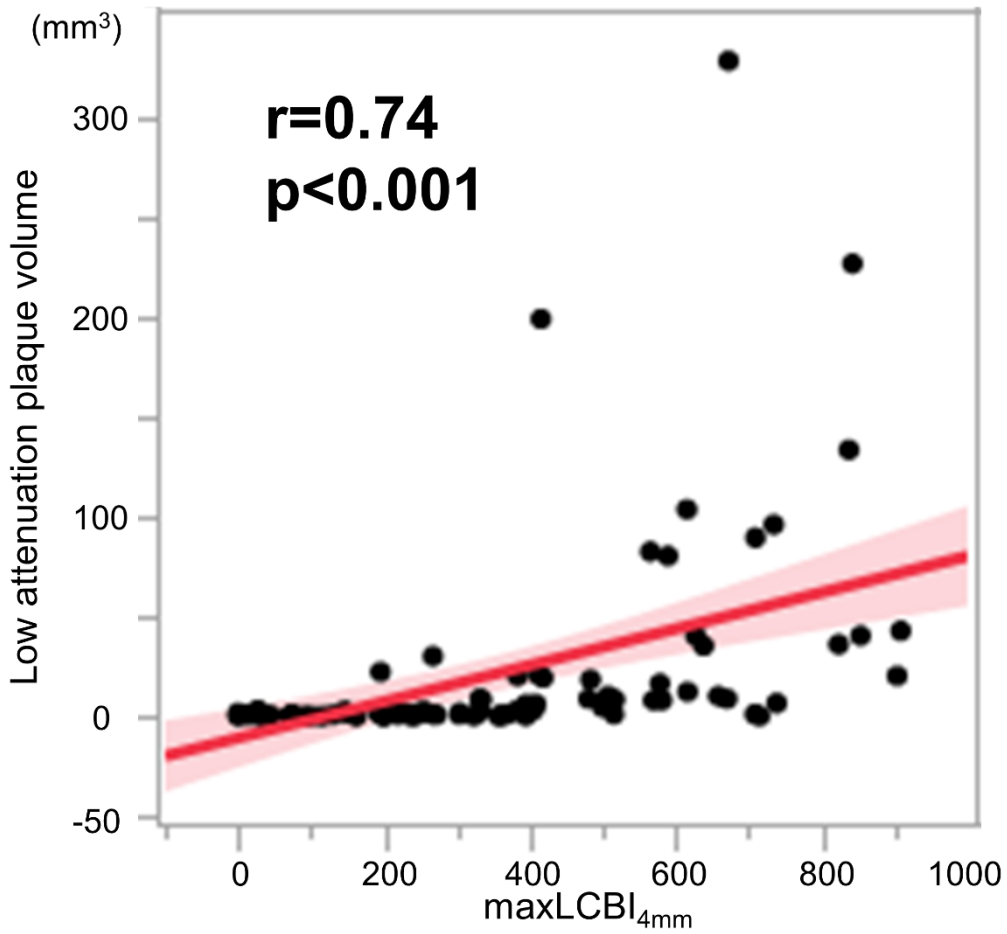

Supplementary Figure 4.

X: $maxLCBI_{4mm}$, Y: CT density